High Carrier Mobility in a Series of New Semiconducting PPV-Type Polymers

Frederik C. Krebs* and Mikkel Jørgensen

The Danish Polymer Centre, RISØ National Laboratory, P.O. Box 49, DK-4000 Roskilde, Denmark

Received November 29, 2002; Revised Manuscript Received March 24, 2003

ABSTRACT: The synthesis and characterization of a series of semiconducting polymers of the polyphenylenevinylene (PPV) type is presented. These new polymers have every second phenylene ring substituted by two alkyl groups of equal length which are hexyl, heptyl, octyl, nonyl, decyl, undecyl, and dodecyl. The polymers were synthesized from the corresponding dialkyldialdehydes by a Horner−Wadsworth−Emmons condensation reaction with 1,4-bis(diethylphosphonomethyl)benzene in a high boiling solvent mixture. The purified polymers were found to have charge carrier mobilities in the range 0.01−0.1 cm^2 V^{-1} s^{-1} and carrier lifetimes of the order of 0.1−5 ms measured by the PR−TRMC technique. A possible explanation for the unexpectedly large magnitudes of both the charge carrier mobility and lifetimes was arrived at by powder X-ray diffraction studies which provided a putative structural model. Finally the electronic structure was studied by ultraviolet photoelectron spectroscopy and the photodegradative properties of thin films of the polymers characterized by illumination through a suitable photopositive mask allowing for subsequent doping giving highly anisotropic conducting patterns.

Introduction

High carrier mobility is an important goal for new organic polymer electronic materials. Intense research effort has allowed for the successful demonstration of semiconductor applications such as field effect transistors[1−3] (FET's), light emitting diodes[4,5] (LED's), photovoltaic devices,[6−9] etc. based on the semiconducting polymer materials currently available. Most of them exhibit very low carrier mobilities and carrier lifetimes when compared to conventional silicon and gallium arsenide counterparts.[10] While it is not expected that semiconducting polymer materials will attain the performance of the inorganic counterparts in terms of carrier mobilities, lifetimes and purity it is of large importance to achieve the highest possible values for these key properties in the semiconducting polymer materials of interest. The fundamental understanding that allows one to achieve high carrier mobility is thus a highly attractive goal. The three most important requirements can be identified as the structure, an extended π-system, and readily accessible carrier states. The latter two factors are intimately linked and can to a large extent be solved by synthetic organic chemistry. The organization and structure of polymer materials, however, are currently very difficult to control, and a large effort within this area is needed. It is the disordered molecular structure in semiconducting polymer materials that is believed to increase the barrier to interchain hopping, which is considered to be the rate-limiting step to carrier transport in molecular and polymer materials. In the present work we have chosen to measure the carrier mobilities by the pulse-radiolysis time-resolved microwave conductivity (PR−TRMC) technique.[11] In this method the semiconducting polymer sample is placed in a microwave reflection cavity and subjected to a short (10−100 ns) electron pulse (from a 10 MeV linear electron accelerator) that create electron/hole pairs. The conductivity change is the measured as the transient absorption of the microwaves using a GHz sampling rate. The PR−TRMC method is contactless, thus avoiding injection barrier problems between electrodes and sample inherent in other methods for measuring carrier mobilities, such as TOF measurements. The PR−TRMC technique measures the maximum trap-free mobilities of carriers in domains of the sample. Bulk mobilities measured by other techniques can be considerably smaller due to domain boundaries and injection barriers.[12] Semiconducting polymers such as the substituted poly(*p*-phenylenevinylene)s (PPV's) and PPV itself have been known for a long time and have proved valuable as materials for the development of polymer electronic devices.[13] It is surprising that most materials studied aside from the parent compound have had alkoxy groups as substituents.[14,15] Few attempts have been made to study the relationship between the molecular substitution pattern and the resulting influence this has on the structure and on the mobility of charge carriers.

Scheme 1. Alk = Linear Alkyl Chains C_6 to C_{12}

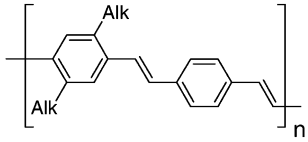

In this paper we present the synthesis and characterization of a series of poly(dialkylstilbenevinylene)s abbreviated dialkyl-PSV's as shown in Scheme 1.

We then explored the material properties of these semiconducting polymers with respect to the charge carrier mobility, charge carrier lifetime, and the electronic energy levels and present a putative structural model based on X-ray powder diffraction data.

Results and Discussion

Synthesis. The synthesis of the monomers was performed as shown in Scheme 2. All of the compounds **1a**−**g** were known[16] and most of the compounds **2a**−**g** were known[16] except **2d**−**f** which were prepared by a Corriu−Kumada coupling of the corresponding alkylmagnesium bromide on 1,4-dichlorobenzene using a $NiCl_2$−dppp catalyst followed by bromination according to the literature.[16] While compound **7c** has been reported in the literature[17] no reaction details were given. The selective metal−halogen exchange on compounds

* Corresponding author. E-mail: frederik.krebs@risoe.dk.

10.1021/ma025893p CCC: $25.00
Published on Web 05/14/2003

Scheme 2

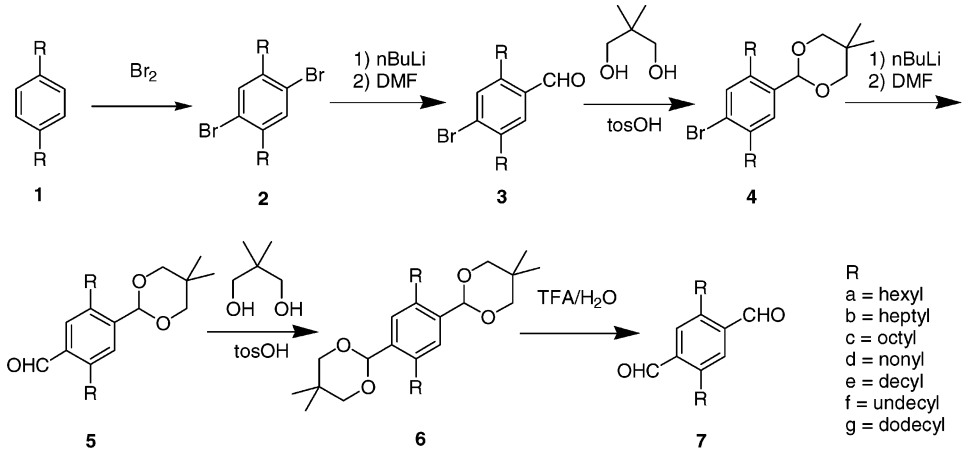

Scheme 3

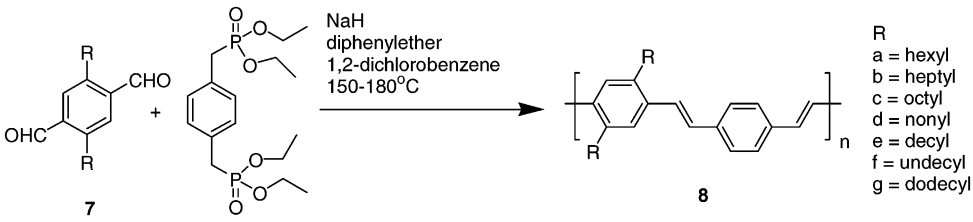

2a−**g** where just one bromine is replaced was not possible without the formation of some impurities that were not easily removed. On the other hand, dilithiation was impossible if a pure product was desired. We found that the reaction sequence where compounds **3a**−**g**, **4a**−**g**, and **5a**−**g** were used directly in subsequent steps without purification gave **6a**−**g** which was easily purified. This could then be deprotected to give **7a**−**g** which was of a high purity suitable for condensation polymerization reactions.

Polymerization. The polymerization reactions were performed using sodium hydride as base in a high boiling solvent mixture as shown in Scheme 3. This was found to give the highest molecular weights.

The raw polymer products were then subjected to Soxhlet extraction with THF for 24 h to remove low-molecular weight material and finally recrystallized/reprecipitated from boiling 1,2-dichlorobenzene. The polymers **8c** and **8d** were of the highest molecular weight, but common to all the polymers obtained was a very broad distribution of molecular weights. In our hands it was not possible to control the dispersity of the polymer product using this mode of polymerization. We initially thought that the co-crystallized solvent water molecules in the compounds **7a**−**g** was responsible for the variation in dispersities observed but removal of this water either by azeotropic distillation before adding the sodium hydride to the polymerization mixture or by dissolving in chloroform and drying the solution gave the same results. We ascribe the variation in molecular weight distributions observed to be governed by small errors in the mixing of stoichiometric amounts of the monomer components and the solubility of the final polymer product under the reaction conditions.

Charge Carrier Mobilities. The minimum sum of carrier mobilities was determined using the pulse radiolysis time-resolved microwave conductivity technique (PR−TRMC) developed by Warman et al.[18,19] The technique is very useful to the polymer scientist looking for new materials with high mobilities and long carrier lifetimes as the method is contactless and thus independent of experimental parameters such as sample preparation (i.e., thin films), sample orientation/organization, domain boundaries, and contact problems such as electrode contact resistance. We have applied this method on a general basis for the screening of newly synthesized materials and selecting materials with high mobilities and long lifetimes. The desirable charge carrier properties of the particular materials presented here were thus discovered by the standard use of this technique. The technique relies on the measurement of a change in reflected microwave power from a polymer sample upon passage of high-energy electrons. From the transient changes in conductivity the lifetime of the carriers can be determined as well as the sum of the mobility of the carriers. The setup used in this work has the sample in a reflection cell measuring the reflected microwave power P_r and the difference in reflected microwave power ΔP (before and after irradiation with an electron pulse). Warman et al. found an expression that relates the maximum of the ratio $\Delta P/P_r$ to the change in conductance ($\Delta\sigma$) of the sample due to the radiation-induced carriers according to eq 1 under the assumption that the medium is isotropic.

$$\left(\frac{\Delta P}{P_r}\right)_{max} = -\Delta\sigma \frac{2\lambda_{vac} f_{max} d}{\epsilon_o c^2}, \quad f_{max} = \frac{c}{2\sqrt{\epsilon_r}}\left[\left(\frac{2n+1}{2d}\right)^2 + \left(\frac{1}{a}\right)^2\right]^{1/2} \quad (1)$$

$$\sum \mu_{min} = \frac{\Delta\sigma}{e(N_+ + N_-)}, \quad N_+ + N_- = \frac{D}{E_p} \quad (2)$$

$\Delta\sigma$ is thus related to the length of the sample, d, and the frequency at which the maximum response is observed, f_{max} (i.e., the largest ratio of $\Delta P/P_r$). From this the sum of carrier mobilities can be obtained since the conductance is the product between the former and the number of carriers ($N_+ + N_-$), which is known from

Table 1. Sum of Carrier Mobilities Measured by PR−TRMC[a]

compound	$\Sigma\mu_{min}$ ($m^2\ V^{-1}\ s^{-1}$)	τ_1 (ms)	τ_2 (ms)	M_p
8a	1.28×10^{-6}	0.1517	2.628	13 500
8b	5.78×10^{-6}	0.3994	4.843	3280
8c	9.14×10^{-6}	0.3926	4.295	26 400
8d	8.90×10^{-6}	0.5284	6.017	129 000
8e	6.12×10^{-6}	0.2586	3.245	29 100
8f	1.87×10^{-6}	0.1873	2.623	9470
8g	4.18×10^{-6}	0.2209	2.576	49 500

[a] The $\Sigma\mu_{min}$ values are based on a carrier pair formation energy of 25 eV. The first and second half-lives τ_1 and τ_2 for the materials studied are also shown. The M_p values obtained from the SEC measurements are also shown.

dosimetry according to eq 2. (see Experimental Section). It is reasonable to assume that the isotropic condition is valid since the powdered and randomly oriented sample completely fills the waveguide and the high energy electrons interact weakly with the material (large penetration depth). The number of carriers is derived from D/E_p where D is the measured dose and E_p is the electron/hole pair formation energy. A value of 25 eV for E_p has been used extensively in previous PR−TRMC studies.[20−25] Alternatively the value of E_p can be estimated from a weighted sum of the electronic band gap for the constituents (i.e., backbone and side chains) of the molecules based on a model by Alig et al.[26] and used in the interpretation of PR−TRMC results.[27−29] For our results presented in Table 1 an E_p value of 25 eV has been used. When deriving an E_p value based on the Alig-model for our systems a lower value for E_p is obtained (i.e., $E_p \sim 15$ eV for **8c**) thus corresponding to a reduction of the mobilities to 60% of the values given in Table 1. The major advantage of the technique is that the magnitude of the carrier mobility obtained is the minimum average carrier mobility within a domain and it is independent of sample preparation, i.e., no contact resistance.

This means that even higher mobilities within individual domains along certain directions is possible as documented for columnar discotic liquid crystals where the mobility along the columnar stack is significantly larger than the minimum sum of mobilities. A disadvantage is that it is the sum of carrier mobilities that is obtained and the technique does thus not allow for distinguishing between hole and electron mobilities except for one specific example.[27] The general results for the polymers **8a**−**g** are presented in Table 1 for thermally annealed samples.

It is noteworthy that the observed magnitudes of the carrier mobilities observed are much larger, by 1−3 orders of magnitude, than for other PPV derivatives[20,28] and larger than for polythiophenes by 1 order of magnitude.[21,29] Values similar to ours have been reported recently however.[11] While the values in Table 1 are very high in general and particularly high for polymeric materials, the mobility in the direction of the stacks could be higher by up to a factor of 3 as shown for discotic liquid crystalline materials where the carrier transport is known to be 1-dimensional. The lifetime of the carriers was observed to be in the millisecond range that is much longer when compared to lifetimes observed for alkoxysubstituted PPV derivatives.[20]

The decays were all nonmonoexponetial and a fit was obtained by using two half-lives as shown in Figure 2. These data are also presented in Table 1. The purification step whereby the polymer materials were recrystallized/reprecipitated from boiling 1,2-dichlorobenzene

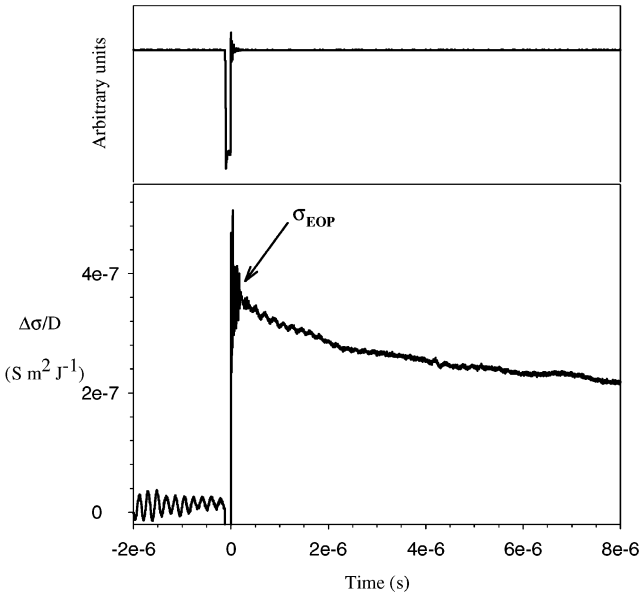

Figure 1. PR−TRMC dose normalized transient (below) showing the end-of-pulse conductivity value, σ_{EOP}, that was used to extract the minimum sum of carrier mobilities, μ_{min}, in Table 1 for polymer **8d**. Above, the 100 ns electron pulse that creates the carriers is shown (recorded with a Faraday cup after passage through the sample).

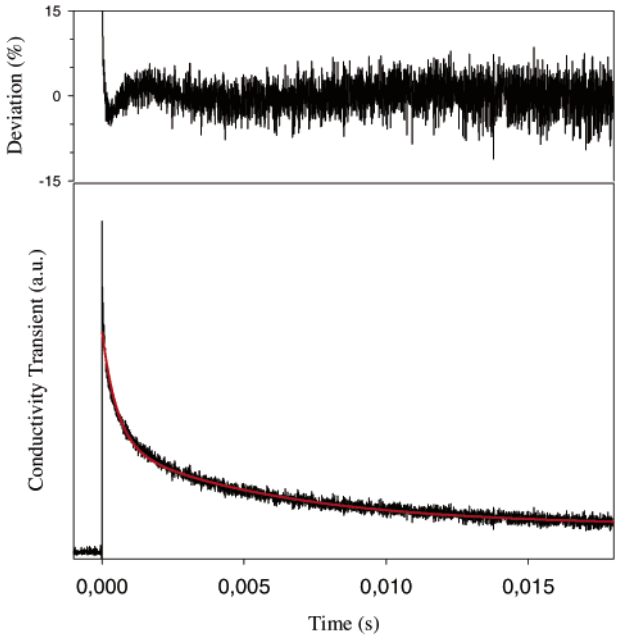

Figure 2. Very long conductivity transient for the polymer **8d** recorded using a slow sampling rate of 2.5 Ms s^{-1} to monitor the conductivity decay in the millisecond range. The biexponential fits according to the carrier lifetime values given in Table 1 are shown. The difference between the data and the fitting function is shown at the top as the percentage deviation.

had little influence on the magnitude of the carrier mobilities. However, the lifetimes of the carriers was increased by a factor of 10^3. These very large values of carrier mobilities and the long lifetimes led us to attempt studying the structure and organization of the recrystallized/reprecipitated materials by powder X-ray diffraction.

Structural Model. It seemed puzzling that these materials should exhibit such high values for the mobility when compared to the known PPV derivatives which almost exclusively has alkoxy substituents and

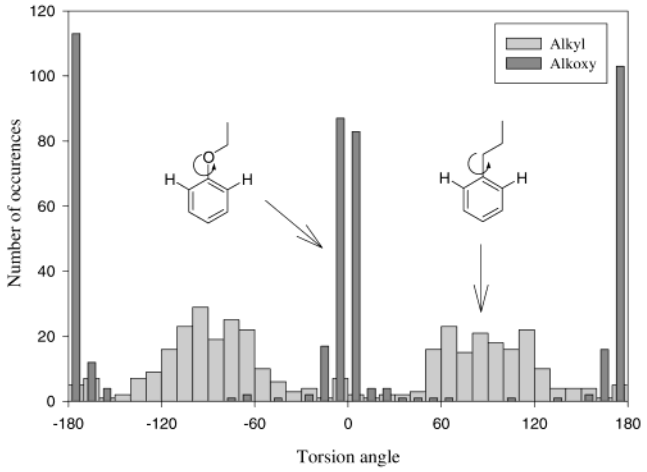

Figure 3. Number of occurrences in the CSD of structures in a given 10° torsion angle span for, respectively, alkyl− and alkoxy−aryl compounds with search fragments shown as insets. There were 365 alkyl occurrences and 457 alkoxy occurrences.

a substitution pattern that has every phenylene unit substituted. We started by considering the typically observed behavior of the substituents in the solid state by use of the Cambridge Structural Database[30] (CSD) which contains a wealth of information on the structure of molecular organic materials. By searching the database for the geometries of selected molecular fragments, we succeeded in identifying striking differences in the conformational behavior of substituents generally employed in semiconducting polymers.

Most significantly the torsion angle span observed between an aromatic system and a substituent revealed that alkyl and alkoxy groups are orthogonal as shown in Figure 3.

This essentially implies that the methylene group directly attached to a benzene ring prefers a torsion angle of about 90° while it is about 0° for similar alkoxy substituents as shown in Figure 3. The total number of occurrences in the CSD for respectively alkyl- and alkoxy-substituted aryl compounds of the type indicated by the search fragments were similar. It is evident that the torsion angles for alkyl groups are more relaxed and a larger conformational range is available. These preferences are undoubtedly responsible for the differences in packing properties of dialkyl- vs dialkoxy-substituted polymers. We used this information to obtain a reasonable starting model for our powder diffraction studies and also solved the structure of compound **6c** to further substantiate these findings. The molecular structure for **6c** is shown in Figure 4 where a torsion angle between the benzene ring and the innermost methylene group is close to 90° as expected.

Recent studies of model compounds for alkyl- and alkoxy-substituted polyparaphenylenevinylenes presented single-crystal X-ray data and molecular structures observed are consistent with our results.[31,32]

X-ray powder diffraction on the polymers **8a**−**g** (see also Supporting Information) performed in this study showed that the alkyl substituted PPV's had a reasonably degree of crystallinity and many Bragg peaks were observed. Considering the very rigid nature of the polymer this led us to try and model the crystal structure from powder data on annealed samples of the material by rigid body refinement and finding support for our initial structural model through the CSD-search shown in Figure 3 but also a search on *trans*-stilbenes.

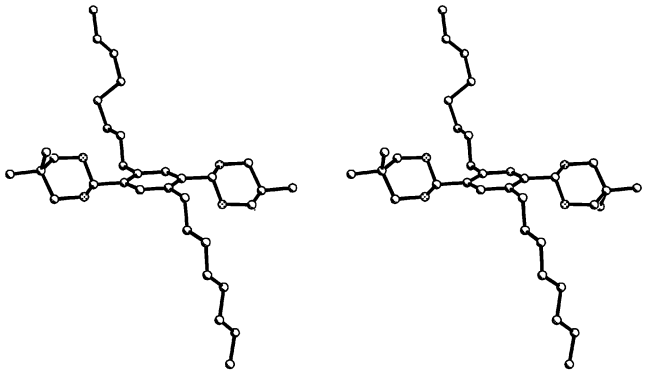

Figure 4. Stereoview of the diacetal **6c** showing how the alkyl groups form a torsion angle with the benzene ring close to 90 °.

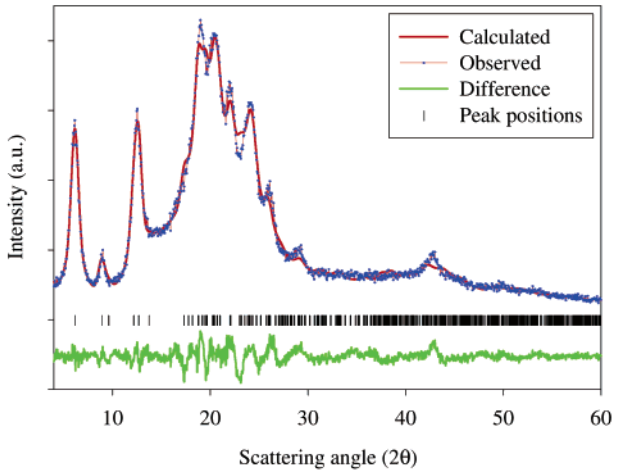

Figure 5. Observed (blue), calculated (red), and difference (green) plot for **8c**. The powder data were acquired on samples annealed at 150 °C for 24 h under argon using Cu Kα radiation.

Several initial models were attempted, and all converged on a solution where the experimental powder diffractogram and the calculated powder diffractogram were in good agreement as shown in Figure 5. Our putative model obtained in this way show that the polymer PPV backbone of alternating benzene rings and vinylene groups run along the space diagonal of the triclinic unit cell. This arrangement maximizes the overlap between the polymer chains, which in turn facilitates high carrier mobility. The main finding is that the stacking of the stilbene units is eclipsed giving rise to near maximum π-overlap as shown in Figure 6. The alkyl chains gives rise to an interdigitating pattern that cause the structure to become layered. The extended sheets of the PPV backbone that are isolated by the alkyl chains probably hold the explanation to the long carrier lifetime that is only surpassed by a few columnar discotic liquid crystal materials where such large carrier lifetimes and mobilities have been observed.[25] For our materials there is no significant correlation between the magnitude of the observed lifetimes and the alkyl chain length. We ascribe this to a more 2-dimensional transport mechanism giving conduction paths both along the polymer chains, but also between the chains due to the good overlap. In the case of poly(3-alkylthiophene)s a correlation between alkyl chain length and carrier lifetime has been observed.[29] One aspect of the values in Table 1 is the lack of correlation between the alkyl chain length and the carrier mobility and lifetime. For

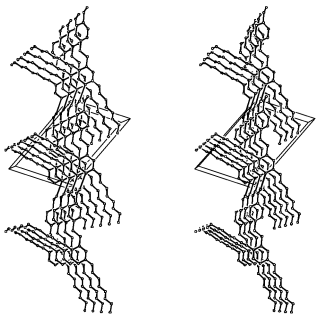

Figure 6. Stereoview of the putative structural model obtained from the powder X-ray diffraction data for **8c**. The polymer strands are stacked in sheets with the alkyl chains surrounding them. Every second vinylene group forms torsion angles significantly different from 0° forcing the intermolecular $\pi-\pi$ interactions to be eclipsed. One alkyl chain extends above the plane of the polymer strand and the other alkyl chain extends below the plane of the polymer strand.

the discotic liquid crystal materials studied using the PR−TRMC technique there is a strong correlation between alkyl chain length and the carrier lifetimes. This observation has been rationalized through the insulating nature of the alkyl chain core for these highly 1-dimensional systems. Aside from the possibility of a more 2-dimensional nature of the conduction paths in our materials as mentioned above, there are at least four important issues. First, the molecular weights vary considerably between the samples studied. Second, the most crystalline samples (see Supporting Information) generally have the highest values for both carrier mobility and lifetime (i.e., **8a** and **8f** are the most weakly scattering samples and they both have the shortest lifetimes and smallest carrier mobilities). Third, there seems to be a maximum around **8c** and **8d** where the number of side chain atoms approximate the number of backbone atoms and this might be important for the efficient packing with respect to carrier transport. Fourth, we only present the minimum sum of carrier mobilities and have not for instance corrected for the dimensionality, the differential dose distribution (between side chain and backbone), and the carrier pair survival probability, which has been assumed to equal 1 (i.e., 100% carrier pair survival probability). With respect to this last point, an attempted correction using any of these terms would only increase our observed value for the sum of carrier mobilities. We have thus provided a conservative set of values for the carrier mobilities for the compounds **8a**−**g**.

The model obtained this way should be considered with some caution. In particular, the difference between calculated density (0.833 g cm^{-3}) and the density found experimentally (0.95 g cm^{-3}) for polymer **8c** is quite large. The magnitude of the density is however not unreasonably low for a polymer material. We cannot provide a solid explanation for this discrepancy but tentatively ascribe it to the few degrees of freedom in our simple model that however does fit the experimental diffraction data quite nicely. While our putative model explains the observed materials properties (high carrier mobility and long carrier lifetime) the information contained in the powder diffractogram is limited. The crystallinity observed is high for a polymer material but is very poor when compared to molecular crystals. This puts severe constraints on our ability to draw specific conclusions regarding the detailed geometry of the system. In this manner, the packing arrangement

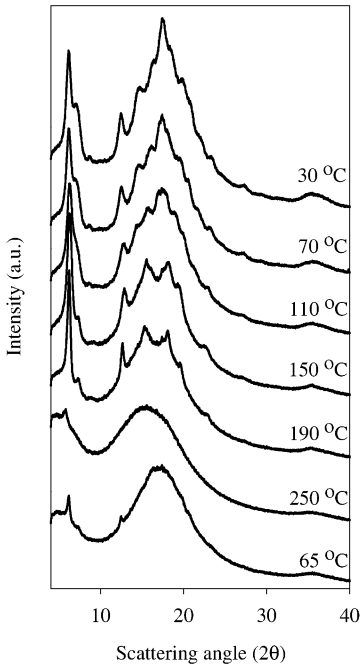

Figure 7. Multiple powder diffractograms collected for compound **8a** upon heating from 30 (top) to 250 °C (second from the bottom). Upon cooling back down to 65 °C, the fine structure of the peaks have disappeared.

illustrated in Figure 6 is very likely to be a good representation. The detailed packing of the alkyl chains, however, is most likely very disordered, and the illustration in Figure 6 should be considered as an effective geometry obtained from the Rietveld refinement.

Thermal Behavior. We chose to obtain further information on the behavior of the alkyl side chains by thermal studies. The DSC data generally showed a transition around 110−130 °C, which is ascribed to side chain melting.[33] The transition was not easily observed for all the compounds and was found to be irreversible if heated above the melting point of the polymers which were generally observed at temperatures in the interval 200−300 °C. In the case of **8a** the side chain melting in the temperature interval 70−150 °C was very difficult to quantitate from the DSC trace. A powder diffraction study using synchrotron radiation however more clearly showed the changes observed in the 70−150 °C interval and the irreversibility when heating above melting (see Figure 7). The use of X-ray powder diffraction for thermal studies turned out to be an alternative method for the establishment of phase changes and confirmed the irreversible melting and subsequent crystallization also observed in the DSC measurements. The fact that the side chain melting or mesophase transition is not reversible (on the time scale of the experiment) if the samples are melted indicates that the desirable high mobility/long lifetime phases are obtained only by recrystallization/reprecipitation of the polymers.

This information is very valuable if devices or studies where one makes use of the desirable materials properties are to be made. We then performed an annealing study also using synchrotron powder X-ray diffraction for **8c** as shown in Figure 8. Here the annealing is shown to alter the diffraction pattern irreversibly (on the time scale of the experiment) while maintaining a high degree of crystallinity when heating above the first transition (to 150 °C) and cooling back down. Upon

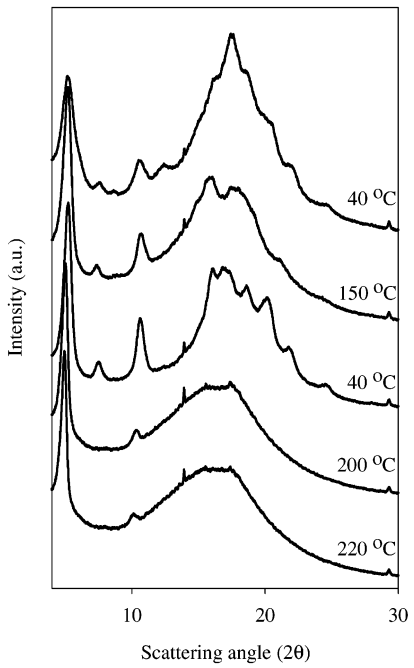

Figure 8. Thermal annealing study for compound **8c** using synchrotron X-ray diffraction. The pristine purified sample (trace shown above) was heated to 150 °C (second trace from the top) and cooled back to 40 °C (middle trace) where some of the peaks have become more pronounced. Finally, heating to 200 and 220 °C (lower traces) led to a merging of the peaks in the 10−20° in 2θ interval into a broad feature.

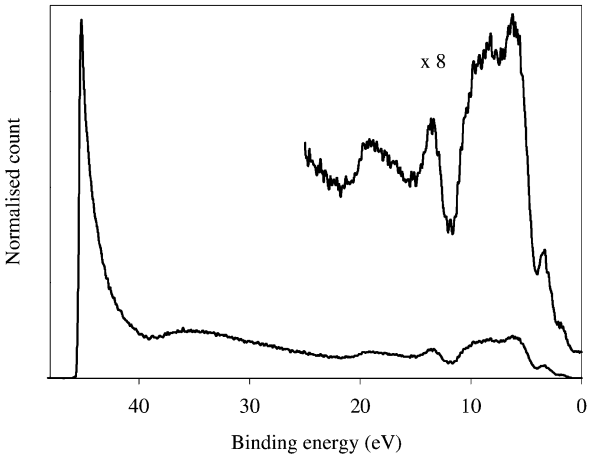

Figure 9. Ultraviolet photoelectron spectrum of the polymer **8c** spin coated on a polycrystalline silver surface using a photon energy of 50 eV. The large signal toward the cutoff at around −46 eV is due to secondary electrons. The reference level is the vacuum level with respect to silver.

heating further (to above 200 °C), the diffraction pattern merged to broad features and the distinct pattern was no longer observed.

Thermogravimetric analysis (TGA) showed that all the polymers decomposed with onset temperatures at around 325 °C and derivative peak decomposition temperatures at around 480 °C. The polymers can thus be considered as quite stable thermally.

Electronic Structure. While high carrier mobilities and lifetimes are suitable for constructing devices the actual application of the material may depend on many other factors relating to the physical construction of the device. Aside from the preparation of films or samples with materials properties identical to the bulk sample the position of the filled energy levels in the context of an electrode material, the optical band gap, and the ionization potential are important materials properties.

Table 2. Conductivities Obtained for the Pristine and Photobleached Films Neglecting Possible Differences in the Mechanisms Conduction (i.e. injection of carriers in the undoped films)

	undoped (Ω^{1-} m^{-1})	doped (Ω^{1-} m^{-1})
pristine	4.0×10^{-6}	1
photobleached	1.6×10^{-7}	5.1×10^{-3}

Table 3. Single Crystal and Powder X-ray Crystallographic Data for 6c and 8c Respectively

study	**6c**	**8c**
formula	$C_{34}H_{58}O_4$	$C_{32}H_{44}$
formula wt	530.80	428.69
cryst syst	triclinic	triclinic
space group	*P*1	*P*1
Z	2	1
a, Å	5.714(2)	5.1900
b, Å	16.601(7)	11.0153
c, Å	17.899(7)	16.8393
α, deg	108.577(7)	63.7905
β, deg	98.008(8)	96.7334
γ, deg	97.567(8)	97.6577
V, Å^3	1565.3(11)	854.16287
ρ, g cm^3 (calcd)	1.126	0.833
ρ, g cm^3 (obsd)		0.95
cryst dimens, mm	0.25 × 0.25 × 0.10	powder
type of radiation	Mo Kα	Cu Kα
wavelength, Å	0.710 73	1.5418
μ, cm^{-1}	0.071	
T, K	120(2)	293(1)
R−P, R−WP (model)	-	0.0512, 0.0665
R−WP (w/over background)	-	0.22
no. of profile points	-	1121
no. of reflcns	-	780
no. of reflcns	19 922	
no. of unique reflcns (with $I > 2\sigma$)	2839	
R_{int}	0.0949	
$R(F)$, $R_w(F^2)$ all data	0.0689, 0.2092	

Table 4. Results from the Photoelectron Spectroscopic Data on Thin Films of the Polymers 8a−g on Polycrystalline Silver

	E_F^{VB}	E_F^{VAC}	cutoff	Δ	IP
8a	0.90	3.80	45.30	−0.40	4.70
8b	1.05	3.45	45.50	−0.75	4.50
8c	0.70	3.95	45.35	−0.25	4.65
8d	0.80	3.85	45.35	−0.35	4.65
8e	0.90	3.75	45.35	−0.45	4.65
8f	1.10	3.50	45.40	−0.70	4.60
8g	0.90	3.80	45.30	−0.40	4.70

The ionization potential, IP, the distance from the Fermi level of the electrode material to the position of the valence band, E_F^{VB}, and distance from the Fermi level of the electrode material to the vacuum level, E_F^{VAC}, were determined using ultraviolet photoelectron spectroscopy (UPS) on thin films of the polymers spin-coated on a silver substrate by procedures described in the literature.[34−36] The ionization potential of the polymers ranged from 4.5 to 4.7 eV (see Table 4). The position of the valence band edge for the polymers, E_F^{VB}, was lower than the Fermi level of silver by about 0.7−1.1 eV. In Figure 9, a photoelectron spectrum of the dioctyl derivative is shown with reference to the Fermi level of silver. The values obtained for E_F^{VB} represents the barrier to hole injection into the valence band and is a reasonable value for electron rich materials such as the materials studied here.

Photodegradation and the Formation of Patterns. We found that irradiation with UV light in air led to the rapid disappearance of the characteristic yellow color of the polymer films. We ascribe this to the

Figure 10. Photoresist properties of dioctyl-substituted polymer. A cast film was irradiated with a 150 W xenon lamp (100 mW cm^{-2}) for 5 min through a positive mask. The result is the image to the left where the exposed part of the film has been photobleached. When the film was then exposed to ICl vapor, the doping gave rise to a dark coloration of the unexposed part of the films.

well-known oxygen dependent photodegradation (a 2 + 2 cycloaddition between the polymer vinylene groups and oxygen).[37] When performing the same experiment in a vacuum of $P < 10^{-7}$ mbar the yellow color persisted with undetectable change in absorbance of the film upon exposure for 24 h. We applied this property as an in-built photoresist.

Thin films of the yellow PPV polymers were spin-coated onto a Pyrex glass slide. A 150 W xenon lamp was used to illuminate the film through a positive mask for 5 min. The exposed areas became colorless, leaving a yellow image of the mask as shown in Figure 10. Doping was then affected with vapors of iodine or more effectively with iodine monochloride. Only the nonirradiated parts changed color to the characteristic blue-black of the charge-transfer complex also shown in Figure 10. The conductivity increase upon doping was very high for the unexposed part of the film. dc-conductivity measurements with and without doping was performed for both pristine and photobleached films. The films were cast from 1,2-dichlorobenzene onto an etched pattern on 10 Ω $square^{-1}$ ITO slides. In Table 2, the results from the experiment are shown.

In the undoped films, the dc conductivity should be treated with caution as the material in this state is semiconducting with very few intrinsic carriers. Upon doping, the behavior becomes ohmic. The conductivity anisotropy is very high between doped and undoped material and is close to a factor of 10^6. The doping anisotropy between bleached and unbleached material is of the order of 10^3. This property could be particularly useful for the simple design of electronic circuitry where a homogeneous film can be patterned after application. It should however be kept in mind that there are many uncertainties associated with these observations as the degree and homogeneity of the doping is unknown. The results show the relative differences between doped/undoped and pristine/photobleached films, whereas the absolute measures are very dependent on the experimental procedure.

Conclusions

In this work, we have presented the synthesis and characterization of a new series of semiconducting polymers based on polyphenylenevinylene which exhibit high carrier mobilities and long lifetimes. This is mainly ascribed to the high degree of crystallinity for these materials and the structural model obtained from powder diffraction experiments. While crystallinity was used to offer a possible explanation for the high values of carrier mobilities and lifetimes the variation in crystallinity along with the variation in the molecular weights was also used to explain the variation in the observed values. The large values for the carrier mobility and lifetime for the materials presented here was established using the PR−TRMC technique that does not provide insight into the individual contributions toward the carrier mobility and lifetime from ordered and disordered domains, both present in the sample. Our results does however provide a firm basis for further study in terms of applications. We have further characterized the thermal behavior, the electronic structure and the photodegradative properties of the materials and applied the ladder properties to make patterns with high conduction anisotropy.

Experimental Section

Synthesis. All reagents were commercially available. Some signals in ^{13}C NMR spectra were missing. This is ascribed to accidental isochrony and was observed for the compounds **2e**, **2f**, **6g**, and **7d**. Compounds **2a**−**c** and **2g** were prepared as described in ref 16.

General Procedure for the Preparation of Compounds 2d—f. The dialkylbenzenes **1d**−**f** were prepared by a Corriu−Kumada coupling as described (also ref 16). Compounds **1d**−**f** (0.2 mol) were each dissolved in dichloromethane (100 mL) and bromine (0.4 mol) was added. The resulting mixtures were kept in the dark to avoid radical bromination of the alkyl side chains. After stirring for 48 h at room temperature, the products were recovered and recrystallized from ethanol.

2d: Colorless needles in 65% yield; mp 44−45 °C. ^1H NMR (250 MHz, $CDCl_3$, 300 K, TMS): δ = 0.9 (t, 6H, CH_3), 1.1−1.4 (m, 24H, CH_2), 1.5−1.6 (m, 4H, CH_2), 2.7 (t, 4H, CH_2), 7.4 (s, 2H, ArH). ^{13}C NMR (63 MHz, $CDCl_3$, 300 K, TMS): δ = 14.8, 23.4, 30.03, 30.05, 30.1, 30.2, 30.5, 32.6, 36.2, 123.8, 134.4, 142.0. Anal. Calcd for $C_{24}H_{40}Br_2 \cdot C_2H_5OH$: C, 58.43; H, 8.68. Found: C, 58.46; H, 8.35.

2e: Colorless microcrystals in 60% yield; mp 55−56 °C. ^1H NMR (250 MHz, $CDCl_3$, 300 K, TMS): δ = 0.9 (t, 6H, CH_3), 1.1−1.4 (m, 28H, CH_2), 1.5−1.6 (m, 4H, CH_2), 2.7 (t, 4H, CH_2), 7.4 (s, 2H, ArH). ^{13}C NMR (63 MHz, $CDCl_3$, 300 K, TMS): δ = 14.8, 23.4, 30.0, 30.1, 30.2, 30.3, 30.5, 32.6, 36.2, 123.8, 134.4, 142.0. Anal. Calcd for $C_{26}H_{44}Br_2$: C, 60.47; H, 8.59. Found: C, 60.53; H, 8.77.

2f: Colorless microcrystals in 70% yield; mp 58−59 °C. ^1H NMR (250 MHz, $CDCl_3$, 300 K, TMS): δ = 0.9 (t, 6H, CH_3), 1.1−1.4 (m, 32H, CH_2), 1.5−1.6 (m, 4H, CH_2), 2.7 (t, 4H, CH_2), 7.4 (s, 2H, ArH). ^{13}C NMR (63 MHz, $CDCl_3$, 300 K, TMS): δ = 14.8, 23.4, 30.0, 30.1, 30.2, 30.3, 30.5, 32.6, 36.2, 123.8, 134.4, 142.0. Anal. Calcd for $C_{28}H_{48}Br_2$: C, 61.76; H, 8.89. Found: C, 61.31; H, 8.95.

General Procedure for the Preparation of 6a—g. The dibromdialkyl compounds **2a**−**g** (0.165 mol) were each dissolved in dry THF (500 mL) and cooled. At −10 °C, the compound crystallizes into a thick mass. The use of a large magnetic bar made stirring of the mixture become possible at lower temperatures. At −60 °C, *n*BuLi in hexanes (110 mL, 1.6 M) was added and the mixture stirred for 15 min. The mixture did not become entirely clear even though all solids dissolved. Dry DMF (25 mL) was added and the mixture allowed to reach room temperature. After 1 h, HCl(aq) (37%, 100 mL) was added and the mixture evaporated until the THF had been removed. The aqueous phase was extracted with ether (3 × 300 mL) and the light yellow ether phase washed with water (500 mL). Drying over $MgSO_4$ and evaporation gave an oil. A typical yield of 94% was obtained (on occasion the crude product could be crystallized from 90% ethanol (600 mL)). The crude product was refluxed in benzene (500 mL) containing neopentylglycol (16 g, 0.28 mol, excess) and *p*-toluenesulfonic acid (100 mg) with a water separator. After 5 h, the mixture was cooled and washed with $NaHCO_3$(aq) (1 M, 300 mL) and water (300 mL). Drying with $MgSO_4$ and evaporation gave an oil in a typical yield of 83%. The product from above was dissolved in dry THF (500 mL) and cooled to −70 °C, and *n*BuLi in hexanes (1.6 M, 1.1 equiv) was added. Stirring for 10 min and addition of dry DMF (2 equiv) was performed. The mixture was allowed to reach room temperature. HCl(aq) (37%, 100 mL) was added and the mixture stirred for 2 min. The phases were separated and the organic phase washed with water (200 mL). The organic phase was evaporated without drying to give a yellow oil in a typical yield of 76%. The crude product was refluxed in benzene (500 mL) containing *p*-toluenesulfonic acid and neopentylglycol (2 equiv) with a water separator. After 2 h, the reaction was stopped and the organic phase washed with $NaHCO_3$(aq) (1 M, 300 mL) and water (300 mL) and finally dried and evaporated to give an oil that crystallizes. The oil was dissolved in absolute ethanol (300 mL) and crystallized.

6a: Colorless needles in 56% yield based on **2a**; mp 98−99 °C. ^{1}H NMR (250 MHz, $CDCl_3$, 300 K, TMS): δ = 0.8 (s, 6H, CH_3), 0.9 (t, 6H, CH_3), 1.2−1.4 (m, 18H, CH_2, CH_3), 1.5−1.6 (m, 4H, CH_2), 2.7 (t, 4H, CH_2), 3.6 (d, 4H, CH_2), 3.8 (d, 4H, CH_2), 5.5 (s, 2H, CH), 7.4 (s, 2H, ArH). ^{13}C NMR (63 MHz, $CDCl_3$, 300 K, TMS): δ = 14.8, 22.6, 23.3, 23.9, 30.2, 30.9, 32.3, 32.4, 32.9, 78.6, 100.6, 127.9, 136.8, 138.7. Anal. Calcd for $C_{30}H_{50}O_4$: C, 75.90; H, 10.62. Found: C, 75.90; H, 10.72.

6b: Colorless plates in 53% yield based on **2b**; mp 105−106 °C. ^{1}H NMR (250 MHz, $CDCl_3$, 300 K, TMS): δ = 0.8 (s, 6H, CH_3), 0.9 (t, 6H, CH_3), 1.2−1.4 (m, 22H, CH_2, CH_3), 1.5−1.6 (m, 4H, CH_2), 2.7 (t, 4H, CH_2), 3.6 (d, 4H, CH_2), 3.8 (d, 4H, CH_2), 5.5 (s, 2H, CH), 7.4 (s, 2H, ArH). ^{13}C NMR (63 MHz, $CDCl_3$, 300 K, TMS): δ = 14.8, 22.6, 23.4, 23.9, 29.8, 30.5, 30.8, 32.3, 32.5, 32.9, 78.5, 100.6, 127.8, 136.8, 138.7. Anal. Calcd for $C_{32}H_{54}O_4$: C, 76.45; H, 10.83. Found: C, 76.33; H, 10.96.

6c: Colorless needles in 59% yield based on **2c**; mp 97−98 °C. ^{1}H NMR (250 MHz, $CDCl_3$, 300 K, TMS): δ = 0.8 (s, 6H, CH_3), 0.9 (t, 6H, CH_3), 1.2−1.4 (m, 26H, CH_2, CH_3), 1.5−1.6 (m, 4H, CH_2), 2.7 (t, 4H, CH_2), 3.6 (d, 4H, CH_2), 3.8 (d, 4H, CH_2), 5.5 (s, 2H, CH), 7.4 (s, 2H, ArH). ^{13}C NMR (63 MHz, $CDCl_3$, 300 K, TMS): δ = 14.8, 22.6, 23.4, 23.9, 29.9, 30.1, 30.5, 30.9, 32.3, 32.6, 32.9, 78.5, 100.6, 127.8, 136.8, 138.7. Anal. Calcd for $C_{34}H_{58}O_4$: C, 76.93; H, 11.01. Found: C, 76.91; H, 11.08.

6d: Colorless needles in 62% yield based on **2d**; mp 99−100 °C. ^{1}H NMR (250 MHz, $CDCl_3$, 300 K, TMS): δ = 0.8 (s, 6H, CH_3), 0.9 (t, 6H, CH_3), 1.2−1.4 (m, 30H, CH_2, CH_3), 1.5−1.6 (m, 4H, CH_2), 2.7 (t, 4H, CH_2), 3.6 (d, 4H, CH_2), 3.8 (d, 4H, CH_2), 5.5 (s, 2H, CH), 7.4 (s, 2H, ArH). ^{13}C NMR (63 MHz, $CDCl_3$, 300 K, TMS): δ = 14.8, 22.6, 23.3, 23.9, 30.0, 30.1, 30.2, 30.5, 30.8, 32.3, 32.6, 32.9, 78.5, 100.6, 127.8, 136.8, 138.7. Anal. Calcd for $C_{36}H_{62}O_4$: C, 77.37; H, 11.18. Found: C, 77.36; H, 11.33.

6e: Colorless hairfine crystals in 66% yield based on **2e**; mp 92−93 °C. ^{1}H NMR (250 MHz, $CDCl_3$, 300 K, TMS): δ = 0.8 (s, 6H, CH_3), 0.9 (t, 6H, CH_3), 1.2−1.4 (m, 34H, CH_2, CH_3), 1.5−1.6 (m, 4H, CH_2), 2.7 (t, 4H, CH_2), 3.6 (d, 4H, CH_2), 3.8 (d, 4H, CH_2), 5.5 (s, 2H, CH), 7.4 (s, 2H, ArH). ^{13}C NMR (63 MHz, $CDCl_3$, 300 K, TMS): δ = 14.6, 22.3, 23.1, 23.7, 29.8, 29.9, 30.0, 30.1, 30.3, 30.6, 32.1, 32.4, 32.6, 78.3, 100.4, 127.6, 136.6, 138.4. Anal. Calcd for $C_{38}H_{66}O_4$: C, 77.76; H, 11.33. Found: C, 77.57; H, 11.37.

6f: Colorless microcrystals in 63% yield based on **2f**; mp 93−94 °C. ^{1}H NMR (250 MHz, $CDCl_3$, 300 K, TMS): δ = 0.8 (s, 6H, CH_3), 0.9 (t, 6H, CH_3), 1.2−1.4 (m, 38H, CH_2, CH_3), 1.5−1.6 (m, 4H, CH_2), 2.7 (t, 4H, CH_2), 3.6 (d, 4H, CH_2), 3.8 (d, 4H, CH_2), 5.5 (s, 2H, CH), 7.4 (s, 2H, ArH). ^{13}C NMR (63 MHz, $CDCl_3$, 300 K, TMS): δ = 14.8, 22.6, 23.4, 23.9, 30.0, 30.2, 30.3, 30.36, 30.4, 30.5, 30.9, 32.4, 32.6, 32.9, 78.6, 100.6, 127.8, 136.8, 138.7. Anal. Calcd for $C_{40}H_{70}O_4$: C, 78.12; H, 11.47. Found: C, 78.08; H, 11.57.

6g: Colorless thin needles in 67% yield based on **2g**; mp 85−86 °C. ^{1}H NMR (250 MHz, $CDCl_3$, 300 K, TMS): δ = 0.8 (s, 6H, CH_3), 0.9 (t, 6H, CH_3), 1.2−1.4 (m, 42H, CH_2, CH_3), 1.5−1.6 (m, 4H, CH_2), 2.7 (t, 4H, CH_2), 3.6 (d, 4H, CH_2), 3.8 (d, 4H, CH_2), 5.5 (s, 2H, CH), 7.4 (s, 2H, ArH). ^{13}C NMR (63 MHz, $CDCl_3$, 300 K, TMS): δ = 14.8, 22.6, 23.4, 23.9, 30.1, 30.2, 30.3, 30.35, 30.4, 30.5, 30.9, 32.4, 32.6, 32.9, 78.6, 100.6, 127.8, 136.8, 138.7. Anal. Calcd for $C_{42}H_{74}O_4$: C, 78.45; H, 11.60. Found: C, 78.41; H, 11.80.

General Procedure for the Preparation of 7a—g. Compound **6a**−**g** (20 mmol) was dissolved in trifluoroacetic acid (200 mL), and water (15 mL) was added whereby the clear solution becomes turbid. The mixture was stirred with heating to the boiling point and then left to cool on the stirrer for 1 h. The mixture was then cooled with an ice/acetone bath. Water (100 mL) was then added with vigorous stirring. The product crystallized. After filtering, the crude and wet product was recrystallized from acetonitrile. It was found to be important to use the crude and wet product for the recrystallization. If recrystallized material was subjected to further crystallization or the crude product was dried before recrystallization, this led to degradation of the product. The traces of water/acid present in the crude product were thus found to be imperative for a high purity product. Further all the elemental analysis of the products **7a**−**g** indicated a small water content.

7a: Colorless microcrystals in 51% yield; mp 48−49 °C. ^{1}H NMR (250 MHz, $CDCl_3$, 300 K, TMS): δ = 0.9 (t, 6H, CH_3), 1.1−1.4 (m, 12H, CH_2), 1.5−1.6 (m, 4H, CH_2), 3.0 (t, 4H, ArH), 7.7 (s, 2H, ArH), 10.4 (s, 2H, CHO). ^{13}C NMR (63 MHz, $CDCl_3$, 300 K, TMS): δ = 14.7, 23.2, 29.8, 32.3, 32.5, 33.0, 133.8, 137.4, 144.1, 192.4. Anal. Calcd for $C_{20}H_{30}O_2 \cdot {}^1/_6H_2O$: C, 78.64; H, 10.01. Found: C, 78.72; H, 10.01.

7b: Colorless microcrystals in 81% yield; mp 61−62 °C. ^{1}H NMR (250 MHz, $CDCl_3$, 300 K, TMS): δ = 0.9 (t, 6H, CH_3), 1.1−1.4 (m, 16H, CH_2), 1.6−1.7 (m, 4H, CH_2), 3.0 (t, 4H, ArH), 7.7 (s, 2H, ArH), 10.4 (s, 2H, CHO). ^{13}C NMR (63 MHz, $CDCl_3$, 300 K, TMS): δ = 14.7, 23.3, 29.7, 30.1, 32.4, 32.5, 33.1, 133.8, 137.4, 144.1, 192.4. Anal. Calcd for $C_{22}H_{34}O_2 \cdot {}^1/_6H_2O$: C, 79.23; H, 10.38. Found: C, 79.48; H, 10.39.

7c: Colorless needles in 91% yield; mp 67−68 °C. ^{1}H NMR (250 MHz, $CDCl_3$, 300 K, TMS): δ = 0.9 (t, 6H, CH_3), 1.1−1.4 (m, 20H, CH_2), 1.6−1.7 (m, 4H, CH_2), 3.0 (t, 4H, ArH), 7.7 (s, 2H, ArH), 10.4 (s, 2H, CHO). ^{13}C NMR (63 MHz, $CDCl_3$, 300 K, TMS): δ = 14.7, 23.3, 29.9, 30.1, 30.2, 30.4, 32.5, 33.1, 133.8, 137.4, 144.1, 192.4. Anal. Calcd for $C_{24}H_{38}O_2 \cdot {}^1/_6H_2O$: C, 79.73; H, 10.69. Found: C, 79.30; H, 10.69.

7d: Colorless needles in 96% yield; mp 74−75 °C. ^{1}H NMR (250 MHz, $CDCl_3$, 300 K, TMS): δ = 0.8 (t, 6H, CH_3), 1.2−1.4 (m, 24H, CH_2), 1.5−1.6 (m, 4H, CH_2), 3.0 (t, 4H, CH_2), 7.7 (s, 2H, ArH), 10.4 (s, 2H, CHO). ^{13}C NMR (63 MHz, $CDCl_3$, 300 K, TMS): δ = 14.7, 23.3, 29.9, 30.0, 30.1, 32.5, 33.0, 133.8, 137.2, 144.0, 192.3. Anal. Calcd for $C_{26}H_{42}O_2 \cdot {}^1/_6H_2O$: C, 80.15; H, 10.95. Found: C, 80.05; H, 10.98.

7e: Colorless microcrystals in 97% yield; mp 77−78 °C. ^{1}H NMR (250 MHz, $CDCl_3$, 300 K, TMS): δ = 0.8 (t, 6H, CH_3), 1.1−1.4 (m, 28H, CH_2), 1.5−1.6 (m, 4H, CH_2), 3.0 (t, 4H, CH_2), 7.7 (s, 2H, ArH), 10.4 (s, 2H, CHO). ^{13}C NMR (63 MHz, $CDCl_3$, 300 K, TMS): δ = 14.5, 23.0, 29.7, 29.8, 29.90, 29.92, 29.96, 32.2, 32.3, 32.7, 133.5, 137.1, 143.8, 192.1. Anal. Calcd for $C_{28}H_{46}O_2 \cdot {}^1/_6H_2O$: C, 80.52; H, 11.18. Found: C, 80.38; H, 11.18.

7f: Colorless needles in 99% yield; mp 83−84 °C. ^{1}H NMR (250 MHz, $CDCl_3$, 300 K, TMS): δ = 0.8 (t, 6H, CH_3), 1.1−1.4

(m, 32H, CH_2), 1.5−1.6 (m, 4H, CH_2), 3.0 (t, 4H, CH_2), 7.7 (s, 2H, ArH), 10.4 (s, 2H, CHO). ^{13}C NMR (63 MHz, $CDCl_3$, 300 K, TMS): δ = 14.8, 23.4, 30.0, 30.1, 30.2, 30.23, 30.3, 30.31, 32.5, 32.6, 33.1, 133.7, 137.4, 144.1, 192.4. Anal. Calcd for $C_{30}H_{50}O_2 \cdot {}^1/_6H_2O$: C, 80.84; H, 11.38. Found: C, 81.06; H, 11.45.

7g: Colorless microcrystals in 99% yield; mp 84−85 °C. ^{1}H NMR (250 MHz, $CDCl_3$, 300 K, TMS): δ = 0.8 (t, 6H, CH_3), 1.1−1.4 (m, 36H, CH_2), 1.5−1.6 (m, 4H, CH_2), 3.0 (t, 4H, CH_2), 7.7 (s, 2H, ArH), 10.4 (s, 2H, CHO). ^{13}C NMR (63 MHz, $CDCl_3$, 300 K, TMS): δ = 14.8, 23.4, 30.0, 30.1, 30.2, 30.23, 30.3, 30.33, 30.36, 32.5, 32.6, 33.1, 133.8, 137.4, 144.1, 192.4. Anal. Calcd for $C_{32}H_{54}O_2 \cdot {}^1/_6H_2O$: C, 81.12; H, 11.56. Found: C, 81.16; H, 11.62.

General Procedure for the Preparation of the Polymers 8a—g. The dialdehyde **7a**−**g** (5 mmol) was dried at 40 °C in a vacuum oven for 24 h and then mixed with the diphosphonic acid ester (5 mmol) in a 1:1 mixture of 1,2-dichlorobenzene and diphenyl ether (150 mL), and the mixture was degassed with argon. NaH (1 g) was added, and the mixture was refluxed under argon with an air condenser for 24 h. The mixture rapidly acquires a cloudy yellow/green coloration. The mixture was cooled and methanol (200 mL) containing HCl(aq) (37%, 25 mL) was added and the mixture was stirred for 30 min. An additional portion of methanol (1 L) was added and the crude product filtered and washed with methanol. The crude yellow/orange product was then transferred to a Soxhlet extraction apparatus and extracted with THF overnight. The extract contained low molecular weight material. The contents of the extraction thimble was boiled with stirring under argon in 1,2-dichlorobenzene (100 mL) after 2 h the boiling solution was filtered through glass wool to give a clear bright yellow solution that was left to cool slowly under argon. The product forms a gel, and the contents of the flask were poured into methanol (1 L) with vigorous stirring. The yellow product was filtered and dried in the oven at 90 °C for 24 h.

8a (dihexyl-PSV): Dark orange polymer in 56% yield. ^{1}H NMR (250 MHz, $C_6D_4Cl_2$, 420 K, TMS): δ = 0.94 (broad singlet, 6H), 1.4−1.55 (m, 12H), 1.82 (broad singlet, 4H), 2.91 (broad singlet, 4H), 7.15 (d, 2H, J = 16 Hz), 7.49−7.6 (m, 8H). SEC: M_p = 13 500; M_n = 5960; M_w/M_n = 3.507. TGA: onset = 351 °C, derivative peak = 480 °C; DSC, mesophase = 125 °C (onset = 100 °C), melting = 266 °C (onset = 242 °C, 2.4 KJ mol^{-1}).

8b (diheptyl-PSV): Bright orange polymer in 40% yield. ^{1}H NMR (250 MHz, $C_6D_4Cl_2$, 420 K, TMS): δ = 0.93 (broad singlet, 6H), 1.36−1.5 (m, 16H), 1.81 (broad singlet, 4H), 2.90 (broad singlet, 4H), 7.15 (d, 2H, J = 16 Hz), 7.5−7.6 (m, 8H). SEC: M_p = 3280; M_n = 3480; M_w/M_n = 3.103. TGA: onset = 340 °C, derivative peak = 480 °C; DSC, mesophase = 123 °C (onset = 104 °C), melting = 224 °C (onset = 218 °C, 0.6 KJ mol^{-1}).

8c (dioctyl-PSV): Bright orange polymer in 25% yield. ^{1}H NMR (250 MHz, $C_6D_4Cl_2$, 420 K, TMS): δ = 0.93 (broad singlet, 6H), 1.34−1.55 (m, 20H), 1.84 (broad singlet, 4H), 2.92 (broad singlet, 4H), 7.15 (d, 2H, J = 16 Hz), 7.5−7.6 (m, 8H). SEC: M_p = 26 400; M_n = 14 000; M_w/M_n = 3.179. TGA: onset = 344 °C, derivative peak = 480 °C; DSC, mesophase = 113 °C (onset = 96 °C), melting = 198 °C (onset = 180 °C, 1.6 KJ mol^{-1}).

8d (dimonyl-PSV): Bright orange polymer in 27% yield. ^{1}H NMR (250 MHz, $C_6D_4Cl_2$, 420 K, TMS): δ = 0.93 (broad singlet, 6H), 1.34−1.56 (m, 24H), 1.84 (broad singlet, 4H), 2.92 (broad singlet, 4H), 7.16 (d, 2H, J = 16 Hz), 7.6−7.6 (m, 8H). SEC: M_p = 129000; M_n = 57 100; M_w/M_n = 11.335. TGA: onset = 334 °C, derivative peak = 480 °C; DSC, mesophase = 191 °C (onset = 173 °C), melting = 326 °C (onset = 309 °C, 1.5 KJ mol^{-1}).

8e (didecyl-PSV): Bright orange polymer in 25% yield. ^{1}H NMR (250 MHz, $C_6D_4Cl_2$, 420 K, TMS): δ = 0.93 (t, 6H, J = 7 Hz), 1.4−1.55 (m, 28H), 1.82 (broad singlet, 4H), 2.91 (broad singlet, 4H), 7.15 (d, 2H, J = 16 Hz), 7.49−7.6 (m, 8H). SEC: M_p = 29 100; M_n = 20 600; M_w/M_n = 2.413. TGA: onset = 326 °C, derivative peak = 480 °C; DSC, mesophase = 186 °C (onset = 169 °C), melting = 319 °C (onset = 297 °C, 2.3 KJ mol^{-1}).

8f (diundecyl-PSV): Bright orange polymer in 23% yield. ^{1}H NMR (250 MHz, $C_6D_4Cl_2$, 420 K, TMS): δ = 0.93 (t, 6H, J = 7 Hz), 1.34−1.6 (m, 32H), 1.84 (broad singlet, 4H), 2.93 (broad singlet, 4H), 7.15 (d, 2H, J = 16 Hz), 7.5−7.6 (m, 8H). SEC: M_p = 9470; M_n = 6470; M_w/M_n = 3.060. TGA: onset = 390 °C, derivative peak = 480 °C. DSC, mesophase = 108 °C (onset = 100 °C), melting = 167 °C (onset = 156 °C, 3.2 KJ mol^{-1}).

8g (didodecyl-PSV): Bright orange polymer in 20% yield. ^{1}H NMR (250 MHz, $C_6D_4Cl_2$, 420 K, TMS): δ = 0.93 (t, 6H, J = 7 Hz), 1.3−1.55 (m, 36H), 1.85 (broad singlet, 4H), 2.93 (broad singlet, 4H), 7.15 (d, 2H, J = 16 Hz), 7.5−7.6 (m, 8H). SEC: M_p = 49 500; M_n = 31 600; M_w/M_n = 2.997. TGA: onset = 327 °C, derivative peak = 480 °C; DSC, mesophase = 110 °C (onset = 100 °C), melting = 197 °C (onset = 175 °C, 3.8 KJ mol^{-1}).

Size Exclusion Chromatography (SEC). SEC was performed in THF at 60 °C using polystyrene standards for molecular weight determination. The polymers were generally not very soluble in THF even at the boiling point. Therefore, the polymer samples were dissolved in boiling 1,2-dichlorobenzene and kept at 150 °C until injected into the SEC system. At concentrations of 1 mg mL^{-1}, the 1,2-dichlorobenzene solutions could be diluted with five volumes of THF at 60 °C without any precipitation taking place (dilution by a factor of 5 roughly corresponds to the dilution of the sample during the SEC experiment).

Differential Scanning Calorimetry (DSC). DSC was performed at 10° min^{-1} temperature gradients in the temperature interval 50−350 °C. It was notable that all the samples exhibited a mesophase transition (side chain melting) and a melting point. When a sample was heated beyond the melting point, subsequent cooling gave rise to a glass.

Thermogravimetric Analysis (TGA). TGA was performed in the temperature interval 25−700 °C to establish the thermal stability of the polymers that were all found to exhibit Gaussian degradion peaks in the 440−520 °C temperature interval with a maximum for all the polymers **8a**−**g** at 480 °C.

PR-TRMC Carrier Mobility Measurements. The technique employed for the determination of carrier mobilities was the well-known pulse radiolysis time-resolved microwave conductivity technique (PR−TRMC). The system used the 10 MeV electron accelerator facility at Risø National Laboratory where short pulses of electrons (10−100 ns pulse length) could be passed through the sample placed in an R-band waveguide (26.5−40GHz). Three microwave sources were employed. A HP8690B Sweeper with a HP8697A 26.5−40GHz module in conjunction with a broadband power amplifier. Two Gunn diode sources in the frequency range 31−35 GHz were employed when possible due to the high power (27 dbm) and low noise obtained. The appropriate microwave source could be switched into the system that consisted of a 26.5−40 GHz HP R532A frequency meter and a 26−40 GHz HP R382A attenuator. Hereafter the microwaves were lead into the first port of a three-port circulator and from the second port to the sample holder that was placed in the path of the electron beam. The sample was evacuated to a pressure of 10^{-5}−10^{-4} mbar using a turbo pump during measurements. The reflected microwave power was again entering the second port of the circulator and taken from the third port through an isolator and a circular waveguide cavity filter (TE_{111} band-pass filter with a bandwidth of 500 MHz). At this point the reflected power could be switched into a power meter (HP432A with a HP R486A thermistor mount) for the absolute measurement of microwave power or directly to a HP R422C Schottky barrier diode with a time response better than 1 ns. At this point the time response of the system is limited by the bandwidth of the cavity filter (∼2 ns). The fast transients were recorded in a 50 Ω system on a 4 Gs/s TDS784C oscilloscope from Tektronix. The electron beam was after passage through the sample picked up by a Faraday cup and the signal from the Faraday cup used as the trigger source for the data collection. Both the conductivity transient and the electron pulse were stored for later analysis. The electron pulse was used to monitor changes in beam current and pulse shape and to get

a measure of the absorbed radiation dose per measured beam current. The conductivity was obtained by using a calibration curve relating the reflected microwave power as a function of detector diode output voltage. To extract the carrier mobility, the number of carriers must be known. This was obtained from dosimetry where radiochromic films were used to get the distribution around the sample holder and inside the sample holder in four depths using polyethylene spacers (this procedure followed the ASTM E1275 standard "Practice for use of a radiochromic film dosimetry system"). A better absolute measure of the dose was obtained using alanine pellets where the dose over the whole volume of the pellet is accurately determined (this procedure followed the ASTM E1607 standard "Practice for use of the alanine-EPR dosimetry system"). The typical dose for a 100 ns pulse was 25 Gy, and the variation in dose over the sample volume was 10%. The value for the end-of-pulse conductivity used in the calculation of the minimum sum of carrier mobilities was obtained 100 ns after the end of the electron pulse to ensure a conservative measurement. An analysis of the conductivity transient gave the carrier half-life, $\tau_{1/2}$. The lifetimes were determined using the F900 program from Edinburg Instruments. A fast data acquisition of 500 MS s^{-1} taking 5000 data points were used for the determination of the first half-life that was taken as the characteristic time constant. For the longer decay times 50 000 data points were recorded at 2.5 MS s^{-1} that was subsequently thinned.

Single-Crystal X-ray Diffraction. A crystals of **6c** was subjected to single-crystal X-ray diffraction. The crystals were drawn directly from the mother liquor, coated with a thin layer of protecting oil and mounted on glass fibers using Apiezon grease and transferred quickly to the cold stream of nitrogen (Oxford Cryostream) on the diffractometer (Siemens SMART CCD Platform). The alkyl chains were found to be disordered and this was treated as two mutually exclusive contributions with a refinement of the sof. An almost complete sphere of reciprocal space was covered by a combination of several sets of exposure frames; each set with a different φ angle for the crystal and each frame covering a scan of 0.3° in ω. Data collection, integration of frame data and conversion to intensities corrected for Lorenz, polarization, and absorption effects were performed using the programs SMART,[38] SAINT,[38] and SADABS.[39] Structure solution, refinement of the structures, structure analysis and production of crystallographic illustrations was carried out using the programs SHELXS97,[40] SHELXL97,[40] and SHELXTL.[41] The structures were checked for higher symmetry, and none was found.[42] In all of the structures H atoms were included in their calculated positions. Crystallographic data (excluding structure factors) for the structure reported in this paper have been deposited with the Cambridge Crystallographic Data Centre as supplementary publication no. CCDC-198729. Copies of the data can be obtained free of charge on application to the Director, Cambridge Crystallographic Data Centre, 12 Union Road, Cambridge CB2 1EZ, U.K. (fax (+44)1223-336-033; e-mail deposit@ccdc.cam.ac.uk).

Powder X-ray diffraction. The polymers diffracted X-rays moderately well at scattering angles up to 45° in 2θ when using Cu Kα radiation (see Supporting Information) using standard laboratory powder diffractometer from STOE. Powder data was collected in from 1 to 60° in 2θ. Powder indexing and structure solution was achieved for **8c** using the *Powder-Solve* module in *ReflexPlus* within the *Materials Studio* package from Accelrys.[43] The powder X-ray data collected for the thermal studies were collected at the I711 beamline at the MAXII synchrotron in Lund, Sweden.[44,45] The setup employed a HUBER G670 imaging-plate Guinier camera and an X-ray wavelength of 1.302 Å, which was the longest possible wavelength with the current beamline setup. Longer wavelengths would have been desirable for these polymer samples as they do not scatter to very high angle and they have large peaks at low angle. A wavelength of 2 Å would thus have spread the diffractogram over a larger span in 2θ.

Density Measurements. In view of the low-density found in the modeling of the powder X-ray diffraction data (0.833 g cm^{-3}) a direct measurement was attempted for two of the polymers (**8c** and **8d**). A few grains of the polymer was covered with a few mL of ethanol (δ = 0.7893 g cm^{-3}) weighed out carefully. Acetic acid (δ = 1.0492 g cm^{-3}) was then added dropwise while weighing the sample and ensuring good mixing, until the polymer grains floated freely in the liquid. The density could then be estimated to be 0.95 g cm^{-3} for **8c** and 0.99 g cm^{-3} for **8d**.

Photoelectron Spectroscopy. The samples for ultraviolet photoelectron spectroscopy measurements (UPS) were prepared by spin-coating a 1 mg cm^{-3} solution of **8a**−**g** in 1,2-dichlorobenzene onto a freshly prepared polycrystalline silver surface. The samples were then dried in a vacuum oven at 50 °C for 24 h with the exclusion of light. The samples were then mounted in the load-lock and kept at a pressure of 10^{-9} mbar. The photoelectron spectra were recorded at the ASTRID storage ring at Aarhus University, Aarhus, Denmark. The beamline consists of an SX-700 monochromator and a hemispherical electron energy analyzer. An ESCA (electron spectroscopy for chemical analysis) of the samples was recorded first to check the cleanliness of the area where the incident photons illuminated the sample and to confirm the presence of carbon and the absence of N, Cl, Na, and P. The photoelectrons were measured at an angle normal to the sample surface. The ESCA scans were performed with 800 eV photons and a resolution of 0.4 eV. The photoelectron spectra were recorded using 50 eV incident photons and a resolution of 0.2 eV. The experimental chamber was equipped with an ion gun, a mass spectrometer and a gas dosing system. The sample holder was electrically isolated from the chamber, and the sample was kept at a potential of −9.5 V relative to the surrounding instrument. This serves to eliminate the contribution from the instrument work function at the low energy cutoff. A clean silver substrate was first entered and sputtered with ionized argon using an emission current of 22 mA and a potential of 3 kV. The sputtering was stopped after 1 h, and subsequent measurements of the silver work function gave the reference value for the work function (Φ_{Ag}, = 4.2 eV). The samples **8a**−**g** on silver substrates were introduced and the photoelectron spectra recorded. The onset and cutoff of the intensity normalized photoelectron spectra were used to compute the work function in the case of the pure silver substrate and the ionization potential and valence band edge in the case of the silver substrates containing the samples. The data are presented in Table 4.

The silver work function, Φ_{Ag}, was determined to be 4.2 eV. The position of the valence band edge for **8a**−**g**, E_F^{VB}, was lower than the Fermi level of silver. The Fermi level in compounds **8a**−**g** are thus situated in the forbidden band gap of the materials and the distance from the Fermi level of the samples to the vacuum level is given by the difference between the ionization potential, IP, and E_F^{VB} giving E_F^{VAC}. The vacuum level shift, Δ, is obtained as: $\Delta = E_F^{VAC} - \Phi_{Ag}$. The vacuum level shift reflects how the molecules orient at the surface giving a dipole layer. The procedure employed in the analysis of the data has been reported.[34,36]

Photodegradation. The photodegradation was measured by irradiation of a thin film of the appropriate polymer spin-coated onto a Pyrex glass slide. The absorbance of the sample was measured before and at intervals during irradiation. The irradiation was done in the wavelength range 400−450 nm with an incident power of 10 mW cm^{-2}. In the atmosphere the photodegradation seemed to take place at all wavelengths below 550 nm and was a rapid process where the large absorption of the polymer material at 430 nm disappeared in less than 2 h as shown in Figure 11.

A similar experiment was performed in the absence of atmospheric oxygen by irradiating the film in the same setup with a vacuum chamber kept at a pressure of 10^{-7} mbar. Films irradiated for 24 h only showed a small degradation of the absorbance of less than 5%. The mechanism responsible for the degradation in the absence of oxygen is likely to involve a 2 + 2 electrocyclic reaction mechanism known from topotactic dimerizations or polymerizations of similar materials. The photodegradative properties could be exploited by using the conductive polymer material itself as a photoresist. Illumination of thin films of the material through a positive mask

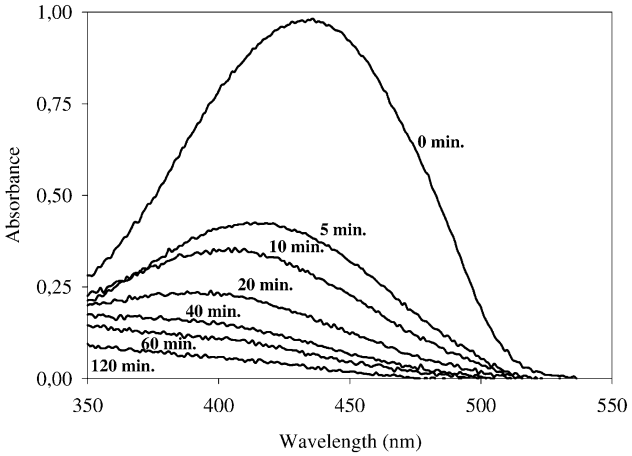

Figure 11. Absorbance as a function of time of a thin film of the polymer **8c** upon irradiation in atmospheric oxygen. The sample was irradiated with 10 mW cm^{-2} in the wavelength range 400−450 nm.

illustrated this. A thin yellow film of the polymer **8c** was irradiated, leading to decoloration of the illuminated area of the film. The film could subsequently be doped with iodine or iodine monochloride, leading to oxidation seen as a darkening of the unexposed area of the film. The conductivity increase upon doping was for the unexposed part of the film very high. The dc conductivity with and without doping was performed for both pristine and photobleached films. The films were cast from 1,2-dichlorobenzene onto an etched pattern on 10 Ω $square^{-1}$ ITO slides. The thickness of the films was measured using a DekTak 3030. Typical values were 150−200 nm. The inter electrode gap was 1 mm.

Acknowledgment. This work was supported by the Danish Technical Research Council (STVF). We would like to express sincere gratitude to Ole Hagemann for technical assistance with the synthetic organic chemistry, Torben Johansen for technical assistance at the Accelerator beamline, Arne Miller and Hanne Corfitzen for the dosimetry measurements, Jan Alstrup for the DSC measurements, Sokol Ndoni and Walther B. Pedersen for SEC measurements, and Zheshen Li, Søren V. Hoffmann, and Philip Hofmann for technical support at the ASTRID storage ring and at the beamline.

Supporting Information Available: A CIF file containing single-crystal structure data for **6c**, Figure S1, showing the ORTEP structure of **6c**, tables showing crystallographic data, atomic coordinates and equivalent isotropic displacement factors, bond lengths and angles, anisotropic displacement factors, and hydrogen coordinates and isotropic displacement factors for **6c**, and Figure S2 showing powder diffraction data for polymers **8a**−**g**. This material is available free of charge via the Internet at http//:pubs.acs.org.

References and Notes

(1) Garnier, F.; Hajlaoui, R.; Yassar, A.; Srivastava, P. *Science* **1994**, *265*, 1684−1686.
(2) Würtner, F. *Angew. Chem.* **2001**, *40*, 1037−1039.
(3) Horowitz, G. *Adv. Mater.* **1998**, *10*, 365−377.
(4) Ciao, Y.; Parker, I. D.; Yu, G.; Zhang, C.; Heeger, A. J. *Nature (London)* **1999**, *397*, 414−417.
(5) Friend, R. H.; Gymer, R. W.; Holmes, A. B.; Burroughes, J. H.; Marks, R. N.; Taliani, C.; Bradley, D. D. C.; Dos Santos, D. A.; Brédas, J. L.; Lögdlund, M.; Salaneck, W. R. *Nature (London)* **1999**, *397*, 121−128.
(6) Granström, M.; Petritsch, K.; Arias, A. C.; Lux, A.; Andersson, M. R.; Friend, R. H. *Nature (London)* **1998**, *395*, 257−260.
(7) Brabec, C. J.; Sariciftci, N. S.; Hummelen, J. C. *Adv. Funct. Mater.* **2001**, *11*, 15−26.
(8) Schmidt-Mende, L.; Fechtenkötter, A.; Müllen, K.; Moons, E.; Friend, R. H.; MacKenzie, J. D. *Science* **2001**, *293*, 1119−1122.
(9) Huynh, W. U.; Dittmer, J. J.; Alivisatos, A. P. *Science* **2002**, *295*, 2425−2427.
(10) Kraft, A. *ChemPhysChem* **2001**, *2*, 163−165.
(11) Warman, J. M.; Gelinck, G. H.; de Haas, M. P. *J. Phys.: Condens. Matter* **2002**, *14*, 9935−9954.
(12) van de Craats, A. M.; Siebbles, L. D. A.; Bleyl, I.; Haarer, D.; Berlin, Y. A.; Zharikov, A. A.; Warman, J. M. *J. Phys. Chem. B* **1998**, *102*, 9625−9634.
(13) Hide, F.; Días-García, M. A.; Schwartz, B. J.; Heeger, A. J. *Acc. Chem. Res.* **1997**, *30*, 430−436.
(14) Wang, H.; Wang, H. H.; Urban, V. S.; Littrell, K. C.; Thiyagarajan, P.; Yu, L. *J. Am. Chem. Soc.* **2000**, *122*, 6855−6861.
(15) Staring, E. G. J.; Demandt, R. C. J. E.; Braun, D.; Rikken, G. L. J.; Kessener, Y. A. R. R.; Venhuizen, T. H. J.; Wynberg, H.; ten Hoeve, W.; Spoelstra, K. J. *Adv. Mater.* **1994**, *6*, 934−937.
(16) Rehahn, M.; Schlueter, A.-D.; Feast, J. W. *Synthesis* **1988**, *5*, 386-388.
(17) Strehmel, B.; Sarker, A. M.; Malpert, J. H.; Strehmel, V.; Seifert, H.; Neckers, D. C. *J. Am. Chem. Soc.* **1999**, *121*, 1226−1236.
(18) Infelta, P. P.; de Haas, M. P.; Warman, J. M. *Radiat. Phys. Chem.* **1977**, *10*, 353−363.
(19) Warman, J. M.; de Haas, M. P. In *Pulse Radiolysis*; Tabata, Y., Ed.; CRC Press: Boca Raton, FL, 1990; Vol. 6, pp 101−132.
(20) Gelinck, G. H.; Warman, J. M. *J. Phys. Chem.* **1996**, *100*, 20035−20042.
(21) de Haas, M. P.; van der Laan, G. P.; Wegewijs, B.; de Leeuw, D. M.; Bäuerle, P.; Rep, D. B. A.; Fichou, D. *Synth. Met.* **1999**, *101*, 524−525.
(22) Schouten, P. G.; Warman, J. M.; de Haas, M. P. *J. Phys. Chem.* **1993**, *97*, 9863−9870.
(23) Warman, J. M.; Schouten, P. G. *J. Phys. Chem.* **1995**, *99*, 17181−17185.
(24) Schouten, P. G.; Warman, J. M.; de Haas, M. P.; Fox, M. A.; Pan, H.-L. *Nature* **1991**, *353*, 736−737.
(25) van de Craats, A.; Warman, J. M.; Fechtenkötter, A.; Brand, J. D.; Harbison, M. A.; Müllen, K. *Adv. Mater.* **1999**, *11*, 1469−1472.
(26) Alig, R. C.; Bloom, S.; Struck, C. W. *Phys. Rev. B* **1980**, *22*, 5565−5582.
(27) Hoofman, R. O. M.; de Haas, M. P.; Siebbeles, L. D. A.; Warman, J. M. *Nature* **1998**, *392*, 54−56.
(28) Remmers, M.; Neher, D.; Grüner, J.; Friend, R. H.; Gelinck, G. H.; Warman, J. M.; Quattrocchi, C.; dos Santos, D. A.; Brédas, J.-L. *Macromolecules* **1996**, *29*, 7432−7445.
(29) van der Laan, G. P.; de Haas, M. P.; Buik, A.; de Ruiter, B. *Synth. Met.* **1993**, *55−57*, 4930−4935.
(30) Conquest Version 1.4 Cambridge Structural Database (CSD), 2002.
(31) Hohloch, M.; Maichle-Mössmer, C.; Hanack, M. *Chem. Mater.* **1998**, *10*, 1327−1332.
(32) Stalmach, U.; Schollmeyer, D.; Meier, H. *Chem. Mater.* **1999**, *11*, 2103−2106.
(33) Bao, Z.; Chen, Y.; Cai, R.; Yu, L. *Macromolecules* **1993**, *26*, 5281−5286.
(34) Krebs, F. C.; Jørgensen, M. *Macromolecules* **2002**, *35*, 7200−7206.
(35) Krebs, F. C.; Jørgensen, M. *Macromolecules* **2002**, *35*, 10233−10237.
(36) Salaneck, W. R.; Lögdlund, M.; Fahlman, M.; Greczynski, G.; Kugler, T. *Mater. Sci. Eng.* **2001**, *R34*, 121−146.
(37) Dam, N.; Scurlock, R. D.; Wang, B.; Ma, L.; Sundahl, M.; Ogilby, P. R. *Chem. Mater.* **1999**, *11*, 1302−1305.
(38) *SMART* and *SAINT. Area-Detector Control and Integration Software;* Siemens Analytical X-ray Instruments Inc.: Madison WI, 1995.
(39) Empirical absorption program (SADABS) written by George Sheldrick for the Siemens SMART platform.
(40) Sheldrick, George M. SHELX-97, Program for structure solution and refinement, 1997.
(41) Sheldrick, G. M. *SHELXTL95*; Siemens Analytical X-ray Instruments Inc.: Madison WI, 1995.
(42) Spek, A. L. *Acta Crystallogr.* **1990**, *46*, C-34.
(43) Engel, G. E.; Wilke, S.; König, O.; Harris, K. D. M.; Leusen, F. J. J. *J. Appl. Crystallogr.* **1999**, *32*, 1169−1179.
(44) Ståhl, K. *J. Appl. Crystallogr.* **2000**, *33*, 394−396.
(45) Cerenius, Y.; Ståhl, K.; Svensson, L. A.; Ursby, T.; Oskarsson, Å.; Albertsson, J.; Liljas, A. *J. Synchrotron Radiat.* **2000**, *7*, 203−208.

MA025893P